

# The mechanical properties of plant cell walls soft material at the subcellular scale: the implications of water and of the intercellular boundaries

M. Shafayet Zamil<sup>1,2</sup> · Hojae Yi<sup>1</sup> · Virendra M. Puri<sup>1</sup>

Received: 5 May 2015 / Accepted: 23 June 2015 / Published online: 7 July 2015  
© Springer Science+Business Media New York 2015

**Abstract** Subcellular mechanical characterization of the cell wall can provide important insights into the cell wall's functional organization, especially if the characterization is not confounded by extracellular factors and intercellular boundaries. However, due to the technical challenges associated with the microscale mechanical characterization of soft biological materials, subcellular investigations of the plant cell wall under tensile loading have yet to be properly performed. This study reports the mechanical characterization of primary onion epidermal cell wall profiles using a novel cryosection-based sample preparation method and a microelectromechanical system-based tensile testing protocol. At the subcellular scale, the cell wall showed biphasic behavior similar to tissue samples. However, instead of a transition zone between the linear elastic or viscoelastic and linear plastic zones, the subcellular-scale samples showed a plateau-like trend with a sharp drop in the modulus value. The critical ranges of stress (20–40 MPa) and strain (5–12 %) of the plateau zone were identified. A strain energy of  $1.3 \text{ MJ m}^{-3}$  was calculated at the midpoint of the critical stress–strain range; this value was in accordance with the previously estimated hydrogen bond energy of the cell wall. Subcellular-scale samples showed very large lateral/axial deformations ( $0.8 \pm 0.13$ ) at fracturing. In addition, investigating the cell wall's mechanical properties at three different water

states showed that water is critical for the flow-like behavior of cell wall matrix polymers. These results at subcellular scale provide new insights into biological materials that possess a structural hierarchy at different length scales; which cannot be obtained from tissue-scale experiments.

## Introduction

With the advancement of molecular spectroscopy, and after decades of study, the structural polysaccharides and the proteins of cell walls have been compositionally and biochemically well characterized [1–5]. However, they also self-assemble into a three-dimensional network of structural constituents, and how they perform as a functional ensemble is not yet well understood. This understanding is pivotal from the perspective of plant cell biology, including for the commercial use of cell wall biopolymers, as well as in materials science and engineering, including of new biomaterials. The microscale size of the cell wall, the nanoscale size and intricate nature of the arrangement of its components, and the interactions between its structural constituents [6] together pose a major hurdle for investigating cell wall architecture and mechanics [7]. Because the mechanical properties of cell walls result from the organization of their structural constituents [8], one way to bridge this knowledge gap is to perform mechanical tests that are designed to investigate the specifics of wall architecture. To date, this indirect method has proven to be a powerful tool to study cell wall functional organization and growth mechanics [2, 8–11].

Due to the technical challenges imposed by the microscale size of cells, the predominant methods for experimentally characterizing primary cell walls are based on

---

✉ M. Shafayet Zamil  
shafayetzamil@gmail.com

<sup>1</sup> Department of Agricultural and Biological Engineering,  
Pennsylvania State University, University Park, PA 16802,  
USA

<sup>2</sup> Present Address: IRBV, University de Montreal, Montreal,  
QC H1X 2B2, Canada

testing macro, or tissue-scale samples [12]. A common experimental protocol at the tissue scale is to chemically degrade [13, 14] or genetically alter [9, 15, 16] a specific structural constituent of the cell wall, then investigate the corresponding changes in the cell wall's architecture and overall mechanics. Sometimes, cutting-edge analytical tools are incorporated, allowing subcellular-scale observations of changes in the arrangement of [17] or interaction between [18, 19] cell wall structural constituents caused by stretching. Despite its successful record as a tool to investigate the cell wall, there are limitations to the use of tissue-scale mechanical tests that need to be addressed.

To test the mechanical properties of the cell wall, the sample should consist only of cell wall materials. The mechanical responses observed from tests on tissue samples are confounded by the effects of extracellular factors such as cell size, shape, distribution, and the middle lamella [20–24]. Thus, tissue-scale mechanical tests are more appropriate for understanding the qualitative nature of the cell wall. In addition, recent cell wall mechanical studies show that pectin may play a major role in maintaining the integrity and growth of the cell wall [25–27]. In addition to their presence in the cell wall, pectic polysaccharides are also abundant in the middle lamella, where they are involved in cell-to-cell adhesion and other biochemical functions [28]. Therefore, tissue-scale mechanical responses are confounded by extracellular factors, including pectin-mediated structural changes in and around the cell wall. Moreover, due to the heterogeneity and distinct hierarchy of biological samples [29], the mechanical responses of tissue samples should be investigated with the caveat that they reflect the bulk or average mechanical properties of an aggregation of cells. Given the aforementioned limitations associated with tissue-scale tests, cell wall characterization at the subcellular level is more appropriate to link the architecture of the cell wall with observed mechanical properties.

Existing technology makes subcellular-scale cell wall characterization a very challenging task. Standard microtensile devices can only accommodate millimeter-scale samples, allowing cellular-level characterization of giant internode cells from algae [30, 31] or single secondary wall fibers [12, 32]. The cells of higher plants are much smaller (micrometer scale), and the extraction of samples from a single cell presents many challenges. Recently, an atomic force microscopy (AFM)-based nanoindentation technique has been used extensively to probe and characterize both primary and secondary cell walls at the subcellular scale [33–35]. The strength of the AFM-based nanoindentation technique is that the samples do not need to be isolated from the tissue; instead, the AFM

tip can scan and characterize samples with nanoscale spatial resolution. This extraordinary capability of nanoindentation-based characterization allows not only investigations of samples at the cellular level, but also experiments on different layers of the cell wall [36]. However, AFM-based characterization is limited to interrogating the force–displacement information orthogonal to the surface of the cell wall or along the thickness of the wall. As a result, the mechanical properties determined using the AFM-based technique require an appropriate mathematical [36] or finite element analysis [37] model with embedded assumptions. To date, the mathematical model developed to interpret AFM force–displacement data for soft biological materials [38] has yet to be optimized for characterizing heterogeneous and multi-layered samples, such as cell walls. To address the intricate architectural nature of the cell wall, an appropriate model needs to be developed.

For quantitative and reliable characterization of the cell wall's mechanical responses, samples need to be extracted and tested at the subcellular scale. Recently, Zamil et al. [39, 40] reported a focused ion beam (FIB)-based sample preparation protocol used in association with a MEMS microextensometer and scanning electron microscope (SEM) image analysis. This method was successfully used to excise a cell wall fragment from the middle of a cell and to conduct experiments under tensile loading conditions. The main advantage of this technique is the capacity for direct mechanical characterization at the cellular level. However, due to the use of the SEM environment for sample preparation and testing, this technique is only suitable for dry samples. The mechanical responses of dry cell walls provided important insights and validated computational models of plant cell wall architecture that do not incorporate water [41, 42]. However, to understand the mechanics and architectural organization of a growing cell wall, it is essential to consider the contribution of water. Water's contribution as a bulk mediator of rigidity changes in major structural polysaccharides of the cell wall; the interactions of these polysaccharides in the presence of water, and, ultimately, to the mechanical responses of the tissue, are well documented and are active areas of research [43–48]. Nonetheless, when all of the cell wall's structural constituents are put together in an intricate functional network, how water changes its mechanics at the subcellular scale is not yet known.

As mentioned above, tissue-scale mechanical properties are representative of average mechanical responses, and they are confounded by extracellular factors and the heterogeneity of cell-to-cell structural arrangements. In this regard, the middle lamella might play a crucial role in

hydration-related cell wall mechanics; both NMR and FT-IR studies of cell wall structural polysaccharides indicate that pectic polysaccharides are more dynamic (less rigid) than other load-bearing components [26, 49, 50] and are major players in maintaining cell wall mobility in water [10, 51]. Thus, to understand cell wall mechanics and architecture with respect to water content, it becomes even more important to extract and test samples without extracellular factors and/or the middle lamella.

This study attempts to mechanically characterize the plant cell wall at the subcellular level under a tensile loading, hydrated environment. The MEMS-based protocol reported by Zamil et al. [39, 40] was further developed using a 3D-printed, adjustable height force sensor to accommodate tests under an optical microscope. This innovation allowed the experiments to be carried out on both non-dried and rehydrated samples using a continuous supply of water. To prepare subcellular-scale samples at near-native state, we used cryotome-based sectioning of the onion epidermal cell wall profile, which is a cluster of open cells that resembles an arrangement of open-topped, joined shoeboxes. The subcellular-scale samples represent a cell wall fragment that consists only of the structural elements, i.e., all extracellular factors and the ML were discarded. Tests were carried out with non-dried and rehydrated samples. The non-dried samples were tested using a silicon chip with an extremely polished surface ( $<1$  nm of root mean square surface roughness), which made it possible to use the stiction force between the sample and the silicon surface to grip the sample. However, stiction does not permit the addition of water during testing, allowing the samples to lose water during the experiments. For tests involving continuous hydration, the samples were gripped using cyanoacrylate glue, and the experiments were carried out with a continuous supply of water using a Nano Mister (Anzikang Nano Handy Mist Spray, Cooskin, Ningbo, China). By analyzing the results of subcellular-scale samples tested under different hydration conditions, along with previously reported dry sample test results [39], we provide a new perspective on cell wall mechanics that cannot be obtained from experiments on tissue-scale samples.

## Materials and methods

### Materials

Fresh white onion (*Allium cepa*) bulbs were bought from a local supermarket. Considering the oldest and outermost fleshy layer as the first scale, the fifth scale was removed

and cut into  $15 \times 5$  mm pieces. The outer epidermis was then peeled off, producing a cell wall profile composed of an open array of epidermal cells resembling an arrangement of open-topped, joined shoeboxes. Onion epidermal peels are well documented to expose cell walls, and they have recently been used to image and characterize the subcellular structural and mechanical properties of the cell wall [39, 40, 52, 53]. The cell wall profile produced from the peel has thick outer epidermal periclinal walls and broken anticlinal side walls. The cell wall profiles from the same scale of the same onion were immediately stored at  $-85$  °C and were used as a consistent source of cell wall material, thereby minimizing biological variability.

### Methods

#### Test setup

The test setup consists of a piezoelectric motor-driven actuator (Model: AG LS25, Manufacturer: Newport, Bozeman, MT, USA) and a 3D-printed force sensor (Proto3000, Vaughan, Ontario, Canada) (Fig. 1a); together, the system functions as a microextensometer. The force sensor beam stiffness was  $24 \text{ N m}^{-1}$ . The displacement resolution corresponds to the resolution of the actuator, which was 440 nm. Based on the displacement resolution of 440 nm, the resultant force resolution was  $13.2 \mu\text{N}$ . Due to the complex shape (3D folded flexure beam) of the force sensor, we calibrated the sensor (i.e., measured the sensor's stiffness) in our lab (Fig. 1b) instead of using the analytical formulation of beam deflection. One of the unique features of this test setup is that the force sensor is attached with an adjustable height micromanipulator (Fig. 1a). The height adjustment mechanism ensures that the very small size of the subcellular-scale sample is in the same plane with respect to both the fixed and moving ends (Fig. 1a). The working principle of this microextensometer is same as that of the microelectromechanical system (MEMS)-based microtensile device [39]. In both cases, an image analysis-based technique was used to measure and calculate the stretching and the applied force exerted on the samples (for detail, please see Zamil et al. [39]). The microextensometer used in this study differs from MEMS-based tensile devices in its force sensor beam design and assembly. A 3D folded type (Fig. 1a) was adapted to make the sensor more flexible, which is a basic requirement for testing soft biological samples. In addition, the sensor was fabricated separately and then assembled with the actuator. The separate force sensor arrangement with adjustable height was very crucial, as it offered sufficient space to manipulate and grip

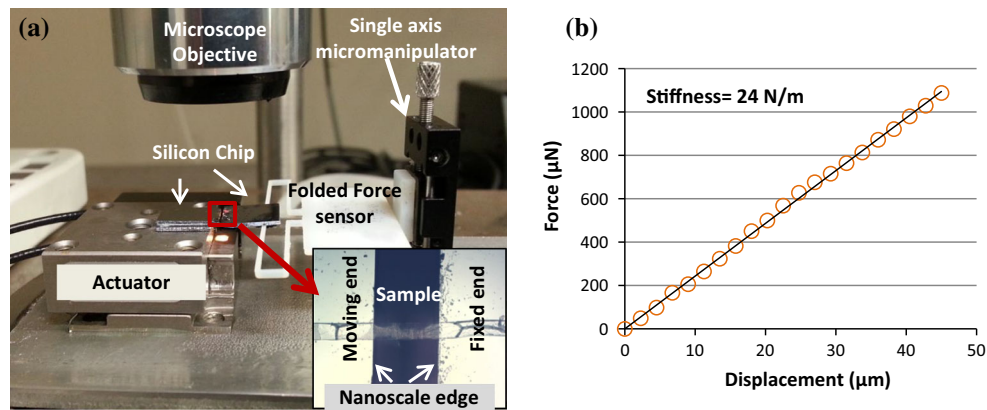


**Fig. 1** **a** Microextensometer setup with a separate folded 3D printed force sensor on adjustable height mechanism controlled by single axis micromanipulator. The actuator is controlled by a voltage source (controller), the single axis manipulator helps keep the actuator side beam (moving end) and the force sensor side beam (fixed end) in the same plane. Two polished silicon chips with nanoscale edges were

attached on both the actuator (moving) and the fixed or force sensor ends. The *inset* shows a sample placed between fixed and moving end. **b** Calibration of folded 3D printed force sensor. The stiffness of the force sensor was calculated as  $24 \text{ N m}^{-1}$  from the slope of the force-displacement data ( $R^2 = 0.99$ )

small-scale biological samples on the device. Another important feature of the setup is the use of a very finely polished silicon wafer cut from a standard silicon wafer (Ultrasil Corporation, Hayward, CA, USA). Two silicon chips were cut using the deep reactive ion etching (DRIE) process. Using cyanoacrylate glue, one chip was attached to the actuator (moving) arm, and other to the force sensor (fixed) arm (Fig. 1a). Thus, the silicon chips became the active moving and fixed end areas of the setup. With sub-nanoscale root mean square (RMS) surface roughness [54], the top surface of the silicon chips facilitated the placement, manipulation, and stiction bonding of submicron-scale cell wall samples in their native state. When the surface of the silicon arms are wet with water, it is possible to maneuver the soft wet sample during preparation without damaging it, as the water interface between the smooth silicon surface and the sample works as a lubricating layer. However, when the water interface dries out, stiction adhesion is activated. The stiction thus produced is the result of nanoscale interactions (hydrogen bonds, van der Waals forces, and electrostatic forces) between the silicon surface and the sample [55]. The DRIE-cut nanoedges of the silicon chips have smooth edges, making it possible to bring the moving and fixed ends of the test device in close proximity. Microscale-sized samples can then be placed and gripped for subsequent mechanical testing.

#### *Native subcellular-scale sample preparation using a cryotome*

To prepare native subcellular-scale samples, the freshly peeled cell wall profile was immediately put into CryoMatrix (Richard-Allan Scientific, Kalamazoo, MI) and

stored at  $-85 \text{ }^\circ\text{C}$ . Using a cryotome, a small patch of the cell wall profile was then cut into 30-micrometer slices. The patch was maintained at a specific orientation during slicing, allowing the major axis of the sample to coincide with the longitudinal direction of a cell that is  $30 \text{ }\mu\text{m}$  wide and a few millimeters long. The details of this sample preparation technique can be found in Zamil et al. [40]. After cryosectioning, the samples were washed and preserved in DI water. Subsequent mechanical experiments were done within 36 h of sample preparation. Samples prepared in this way comprise an array of single cells connected by intercellular boundaries or the middle lamella (Fig. 2a).

#### *Sample pick-and-place and gripping onto the microextensometer test device*

The onion epidermal cell wall section that had been sliced on a cryotome and preserved in DI water (Fig. 2a) was picked using precision tweezers and carefully placed between the fixed and movable ends of the microextensometer, where the chip surfaces had already been wetted with DI water. The samples were precisely manipulated to keep one cell (bounded by two edges of the ML) between the edges of the fixed and movable ends (Fig. 2b). The samples were then gripped such that the effective sample became a fragment of the cell wall within the boundary of a single cell (Fig. 2c). We adopted two different techniques to establish the grip.

1. Gripping with stiction: For native samples that were to be tested immediately after being placed on the device, stiction was used. After placing the sample between the fixed and movable ends of the test device, we



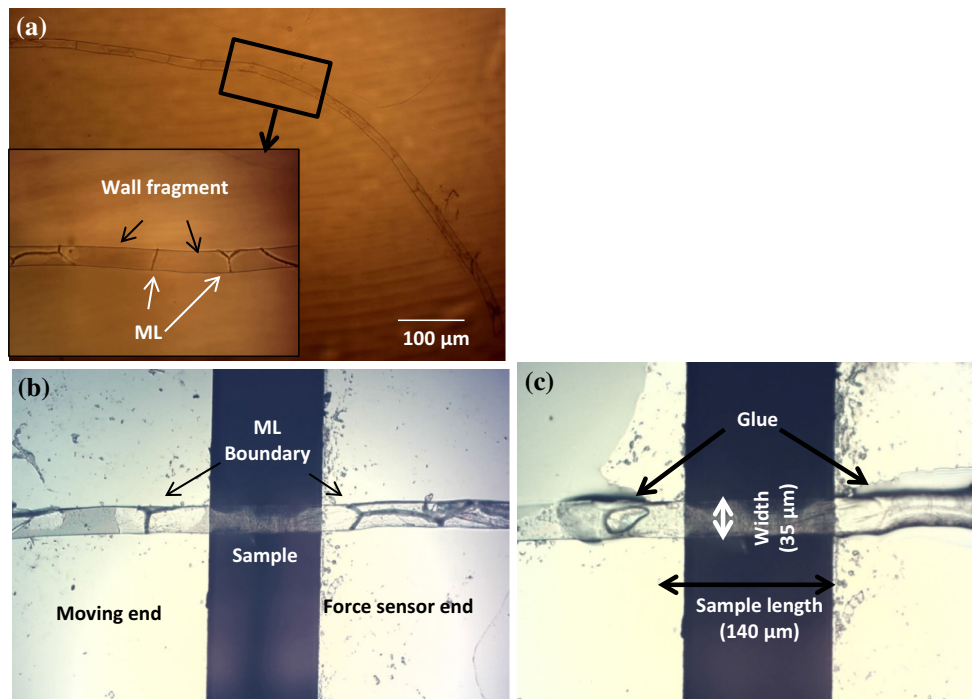
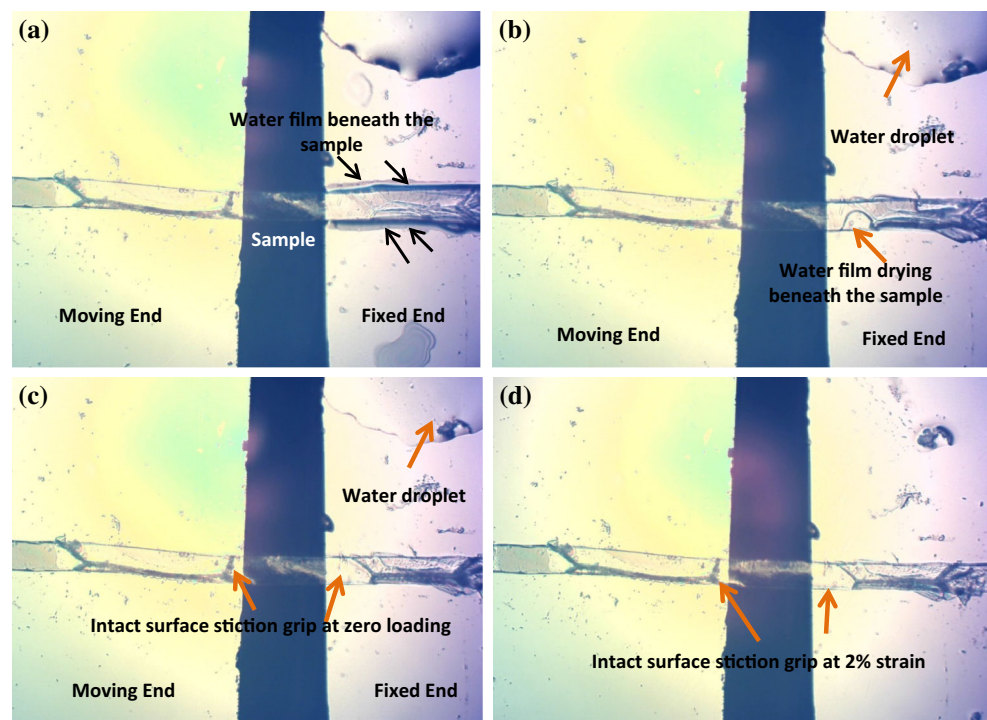


**Fig. 2** **a** Cryotomed onion outer epidermal cell wall slice placed in DI water. The 30  $\mu\text{m}$  wide slice is an array of single cell bounded by ML line in the longitudinal direction. **b** The sample is placed between moving and fixed ends of microextensometer in a way so that only the

fragment of a cell within a cell boundary stays suspended. **c** The grip was established which resulted in effective sample dimensions of 35  $\mu\text{m}$  (width)  $\times$  140  $\mu\text{m}$  (length)

**Fig. 3** **a** The never dried cryotomed sample placed on the smooth silicon surface of moving and fixed ends of the extensometer device. The black arrow shows water film between the sample and the attaching surface. **b** The water film starts to dry out beneath the sample. Time difference between frame (a) and (b) is 4 s. **c** As soon as the water film between sample and the silicon surface dries out, the stiction-mediated grip is established. There are still water droplets around the sample. **d** Stretched sample at 2 % strain. The grip due to stiction force is still intact



allowed the water layer between the sample and the silicon chip to dry out. Once the residual water dried out, the sample and the nanoscale polished silicon

wafer adhered through stiction (Fig. 3c). To our knowledge, this is the first report of the successful use of stiction for thin biological samples. The strength

of the stiction force depends on the roughness of both the substrate and the sample, as well as environmental conditions [55].

- Although this procedure limits the desiccation of the samples, they do experience gradual drying over the course of the experiment. Considering the absence of water during experimentation and the tendency of the microscale samples to dry quickly, the non-dried samples were considered to be in an intermediate water state between that of dry and continuously hydrated samples.
- Gripping with cyanoacrylate glue: To avoid dehydration during the mechanical experiments, continuous rehydration is required. Because the water interface needs to be dried out for stiction-mediated gripping, this bonding was not suitable for mechanical testing of continuously hydrated samples. Therefore, we chose a glue-based gripping technique for experiments using continuously hydrated samples. Gripping with glue required one additional step after sample placement and adhesion to the extensometer surfaces. Immediately after the water at the interface dried out, low viscosity cyanoacrylate glue (Gorilla Glue, Cincinnati, Ohio, USA) was applied to both ends of the sample using a pointed needle. The glue was cured overnight at room temperature with fixed humidity (RH 26 %) to attain sufficient strength for subsequent testing of the continuously hydrated samples.

#### Testing under an optical microscope

**Without continuous hydration** After the samples were placed and gripped with stiction, stretching tests were carried out immediately. The water layer between the sample and the stiction surface was continuously observed to detect the moment of its full evaporation, which indicated that the grip was established. We kept the time gap between grip establishment and the start of the experiment as close to zero as possible. Once the thin film of water starts to dry out at the interface of the sample boundary, the entire drying process completes within a few seconds (Fig. 3b, c). The samples were stretched until any sign of stiction grip detachment, which is easily recognizable in images taken during the experiments. Using a stiction grip, it was not possible to stretch the samples to failure. From the beginning of sample preparation to the initiation of the test, the samples never dried.

**With continuous hydration** For experiments with continuous hydration, samples that had been gripped with cyanoacrylate glue were soaked in DI water for 10 min to re-hydrate them. To prevent dehydration of the samples, moisture was continuously supplied in the form of nanodroplets or mist. We used a Nano Mist spray atomizer

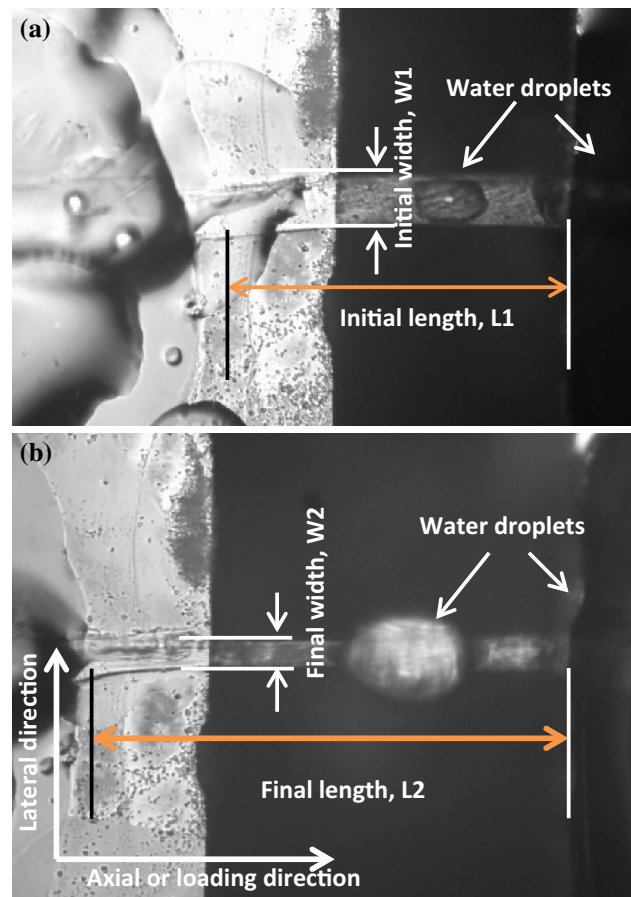


**Fig. 4** **a** Samples at no load condition during mechanical test under continuous hydration.  $L_1$  is the initial length and  $W_1$  is the initial width of the sample. The nanomist of continuous water supply accumulated as droplets on and at the edge of the sample. **b** Sample just before fracture. There is no observable slippage of grip and water droplets are available throughout the experiment.  $L_2$  and  $W_2$  are final length and width of the sample before fracture. Stretching along the loading direction is defined as axial direction and the orthogonal to axial direction is the lateral direction

(Anzikang Nano Handy Mist Spray, Cooskin, Ningbo, China) to spray DI water onto the samples at five-second intervals. The continuous supply of water ensures that the samples are completely wet throughout the stretching test. The samples were stretched from just taut to fracture. Figure 4 shows the presence of water droplets on the sample with no load and just before fracturing.

In both cases (with and without continuous hydration), the samples were stretched at  $1.1 \mu\text{m s}^{-1}$ , and high-resolution images were taken at 1-s intervals throughout the experiment. The images were analyzed using ImageJ (version 1.44p, a Java-based image processing program developed at the National Institutes of Health, USA) to extract the necessary information for mechanical characterization of the samples under tensile loading. The details

of this image-based mechanical characterization technique can be found in Zamil et al. [39].

## Results

### The thickness of non-dried and rehydrated cell walls in situ

Cell wall thickness must be measured accurately because it is an important factor in the overall mechanical response [21]. In epidermal cells, the outer cutinized periclinal walls are frequently thicker than the inner periclinal and anticlinal walls [56]. We adapted a cryo-FIB-based technique for measuring biological specimen thickness that allows the periclinal wall thickness to be directly measured using electron microscopy. The combination of low temperature ( $<-85$  °C), FIB milling, and scanning electron microscopy, along with the cryo-based FIB/SEM FEI Quanta 3D 200 sample preparation and transfer system (Hillsboro, Oregon, USA) was used to cut a trench in the middle of a cell and measure the thickness of the wall at a specific tilt angle of 30°. The details of this technique can be found in [57]. The cryo-based sample preparation and cryo-stage-based FIB technique were adapted so that the sample did not lose water due to vacuum exposure.

The cell wall thicknesses of the non-dried and rehydrated samples were  $1.72 \pm 0.09$  and  $2.05 \pm 0.1$   $\mu\text{m}$ , respectively. These values are in accordance with a previously reported wet sample cell wall thickness (1.65  $\mu\text{m}$ ) measured at the interfacing area between two adjacent cells [58]. A difference between non-dried and rehydrated cell wall thicknesses was observed, which could be due to the inherent biological variability that is observed even among cells in the same tissue (Sokolov et al. [59]; Zdunek and Pieczywek [60]) and/or due to changes in physical properties during the drying and rehydration process. An in-depth analysis of these thickness changes is outside the scope of this study. Our goal was to use an appropriate thickness measurement for both non-dried and rehydrated samples, which was important for quantitative mechanical analysis.

### Stress–strain responses of non-dried samples without continuous hydration

Figure 5a shows the stress–strain responses of wet cell wall samples ( $n = 5$ ) that were never dried but were also not continuously hydrated during the stretching experiment. The stress was calculated by dividing the measured force by the cross-sectional area of the sample, and the strain was

calculated using the measured stretching (deformation) relative to the initial sample length. The cross-sectional area of the sample was the area perpendicular to the direction of stretching, which was measured by multiplying the width and the thickness of the sample. For non-dried samples that were gripped with stiction, we restricted our stress–strain plotting to up to 2 % strain; until this point, the samples showed no visible gripping failure during the tests. In two instances, the samples were able to withstand stretching beyond 2 % strain.

Based on the stress–strain diagram, the average modulus value was  $1.46 \pm 0.2$  GPa. The pooled data from all five experiments (Fig. 5b) also yielded a very similar modulus value of 1.45 GPa, with  $R^2 = 0.90$ .

### The stress–strain responses of wet samples with continuous hydration

Figure 6a shows the stress–strain responses of rehydrated wet samples ( $n = 5$ ). During the entire experiment, from no load to fracture, the samples were continuously hydrated. Because of the large deformation and non-linear trend, each stress–strain diagram contained six equal intervals of 5 % each from 0 to 30 %, plus a seventh interval from 30 % to fracture (Fig. 6b). The modulus value for each interval was calculated separately using linear regression. It was assumed that within each 5 % strain interval, the stress–strain diagram followed a linear pattern. Figure 6c shows the average modulus of the elasticity ( $E$ ) values ( $n = 5$ ) of all samples in each strain interval. The average fracture stress and fracture strain of the five samples were  $81.6 \pm 23.4$  MPa and  $0.45 \pm 0.07$ , respectively.

### Axial versus lateral strain

The axial strain, or simply the strain in the stretching direction, was the measure of the sample's normalized deformation relative to its initial length along the loading direction (Fig. 4). Axial stretching of the sample in the loading direction contracts the sample width in the lateral direction, which is perpendicular to the axial direction (Fig. 7). Similar to the axial strain, the lateral strain was the measure of normalized deformation (contraction) of the sample's width relative to its initial width. Figure 7a shows graphs of lateral strain versus Axial strain for five samples tested under continuous hydration.

We also measured the axial strain ( $A_f$ ) and lateral strain ( $L_f$ ) at the point of sample fracture and calculated a parameter denoted as the LA ratio, which is similar to Poisson's ratio. The LA ratio was defined as follows: (Fig. 4)

Axial strain at fracture ( $A_f$ )

$$\begin{aligned} &= \frac{\text{Final length of the sample before fracture} - \text{Length of the sample at no load}}{\text{Length of the sample at no load}} \\ &= \frac{L_2 - L_1}{L_1} \end{aligned}$$

$$\begin{aligned} \text{Lateral strain at fracture (} L_f \text{)} &= \frac{\text{Final width of the sample before fracture} - \text{Width of the sample at no load}}{\text{Width of the sample at no load}} \\ &= \frac{W_2 - W_1}{W_1} \end{aligned}$$

$$\text{LA (lateral to axial strain ratio at fracture)} = \frac{A_f}{L_f}$$

The LA ratio that we measured was analogous to the well-known Poisson's ratio in materials science. Although the calculation is the same, different terminologies were adopted to avoid confusion with the classical mechanics definition of Poisson's ratio, which has a range of between  $-1$  and  $0.5$ . For an isotropic linear elastic material, Poisson's ratio cannot be more than  $0.5$ . However, where two phases exist, as in the cases of a cellular solid or fiber-reinforced laminate, Poisson's ratio can be much larger than  $0.5$  without violating any physical laws [61, 62]. In such cases, the high anisotropic value between the phases or the deformation of cellular structures in foam helps to attain unusually high Poisson's or LA ratios. In any material, Poisson's ratio largely depends on the microstructural arrangement of its constituent elements [63]. In our case, the pattern of lateral strain over the entire loading step and the corresponding change of modulus values suggested that the higher LA ratio was the result of permanent failure of the matrix polymers, which led to stepwise lateral thinning, the consequences of which are discussed above. The fracture stress, axial fracture strain, lateral fracture strain, and LA ratio were  $81.6 \pm 23.4$  MPa,  $0.45 \pm 0.08$ ,  $0.36 \pm 0.09$ , and  $0.80 \pm 0.13$ , respectively.

#### The mechanical and physical parameters of a typical sample based on instantaneous shape change

One of the unique features of our experimental protocol was the use of high-resolution recorded images at every loading step. These images were used to extract data on stress–strain responses and on three physical parameters of the samples: surface area (length  $\times$  width of the sample), axial strain, and lateral strain. The physical parameters were studied based on instantaneous shape changes, i.e., they were based on the sample dimensions in the prior step instead of the initial dimensions (Fig. 8). Continuously

hydrated samples showed large axial and lateral deformations. Our goal was to investigate if instantaneous shape changes could reveal any additional insight into the stress–strain trend or could be related to observed increases or decreases in modulus values.

The instantaneous stress–strain plots reconfirmed the average stress–strain trend found based on initial sample length (Fig. 6b). In the instantaneous stress–strain plots, the range of the sharp drop in the modulus value was more pronounced (compare Figs. 6b, 8a). The instantaneous surface area, axial strain, and lateral strain were directly measured from images of every loading step. Due to the technical challenges involved in microscale analysis, it was not possible to measure the change in thickness during sample stretching. To simplify, we assumed that the change in thickness during experimentation was negligible and that axial strain mostly led to lateral thinning. Thus, assuming constant thickness, the change in the sample's surface area was representative of the change in its volume during stretching.

## Discussion

### The micromechanical behavior of continuously hydrated samples: a comparison between the cell wall's mechanical properties at the tissue and subcellular scales

Based on micromechanical studies at the tissue scale, the cell wall is modeled as a composite of stiff cellulosic microfibrils embedded in a noncellulosic matrix that exhibits biphasic or bilinear properties [21, 58, 64–66]. These studies recognized two distinctive phases, from which the materials' modulus of elasticity could be measured using the linear trends of stress–strain curves. By testing onion epidermal tissue under tensile loading, Vanstreels et al. [58] and Pieczywek and Zdunek [21] reported



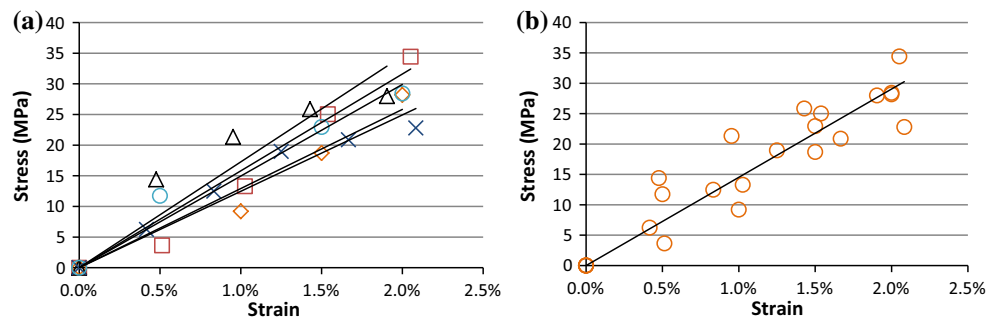


**Fig. 5** **a** Stress–strain diagram of never dried cell wall without maintaining continuous hydration during the test ( $n = 5$ ). The stiction-induced gripping held for tests up to 2 % strain. The *black*

*solid lines* indicate the linear regression of all the five individual samples. **b** stress–strain diagram with linear regression line of the same set of experiments ( $n = 5$ ) for pooled data ( $R^2 = 0.90$ )

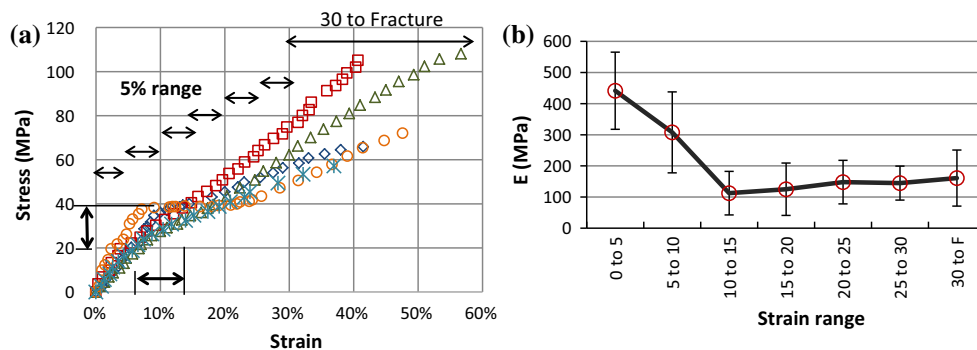


**Fig. 6** **a** Stress–strain diagram of cell wall sample tested under continuous hydration. The *horizontal and vertical two-headed arrows (darker)* indicate the range of axial strain and the range of stress at which the modulus values of the sample drops sharply. For each

sample, the stress–strain plot was divided into seven equal ranges of 5 % strain interval. The modulus of elasticity was calculated in each 5 % interval by linear regression. **b** The average modulus of elasticity corresponding to seven strain ranges

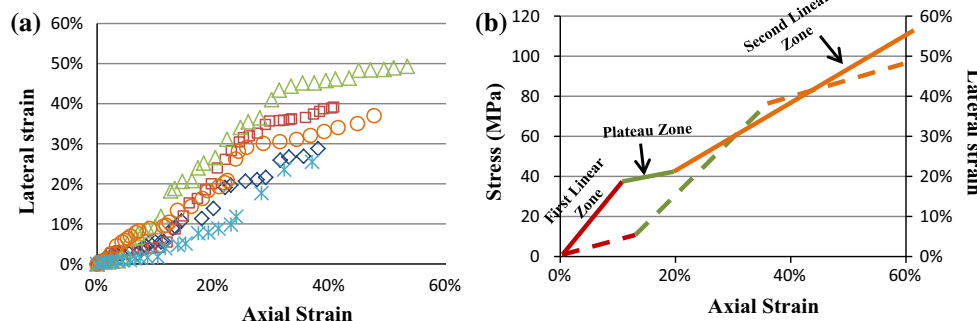


**Fig. 7** **a** Lateral strain versus axial strain of cell wall samples tested with continuous hydration. **b** The average trend of stress and lateral strain against axial strain. The *solid line* denotes stress and *dotted line* denotes lateral strain. The first linear zone (*red line*) was followed by

sharp drop of modulus value denoted as plateau zone (*green line*). After the sharp drop, the modulus value gradually increases, denoted as second linear zone (*orange line*) (Color figure online)

and confirmed a biphasic material model for plant cell walls that had been proposed by Spatz et al. [65] and Köhler et al. [64]. In this model, there is an initial linear elastic or viscoelastic zone, followed by a non-linear transition zone, then another linear zone. In the first linear zone, the cell wall samples' linear elastic responses suggest

that the cellulosic reinforcement and the noncellulosic matrix behave like a classical material, with both the reinforcement and the matrix experiencing the same strain rate. When the material crosses the elastic region, the difference in material properties allows the cellulosic fibers to shear against and break past the noncellulosic matrix

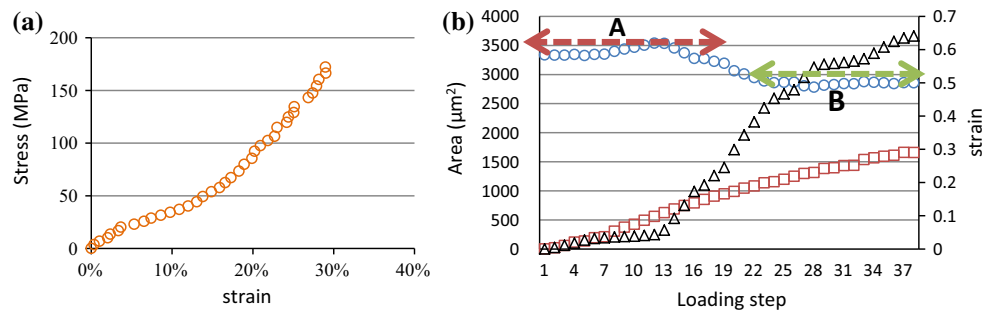


**Fig. 8** **a** stress–strain plot of a typical sample based on instantaneous sample deformation. The plateau zone was more pronounced compared to stress–strain plot based on initial length. **b** The blue circle shows the instantaneous change of surface area for all loading steps. Two same area trends were observed before (dotted two headed

red arrow—A) and after (dotted two-headed green arrow—B) the end of plateau zone. Red rectangle indicates instantaneous axial strain over loading steps, which showed linear increase of strain. Black triangle indicates Instantaneous lateral strain over loading steps showing step-like behavior (Color figure online)

polymers, leading to permanent structural changes in the cell wall. Thus, the second, lower modulus value likely represents irreversible plastic deformation.

The average stress–strain trend of the samples (Fig. 7b) was similar to that of the biphasic material model discussed earlier. At the subcellular scale, we also identified three different zones: (a) the first linear elastic zone, (b) a zone with a large, sharp drop in the modulus value, hereafter referred to as the plateau zone, and (c) the second linear zone, which has a lower modulus value than the first linear zone.

*The first linear zone*

In the first linear zone, the cell wall samples behaved linearly up to approximately 10 %, which is similar to the tissue-scale responses reported by Pieczykew and Zdunek [21] and Vanstreels et al. [58]. However, the average modulus of elasticity value that was calculated at the subcellular scale ( $374.6 \pm 138.8$  MPa) was approximately one order of magnitude higher than that of the tissue-scale experimental results (<60 MPa). The scale of the investigation plays a large role in explaining this difference in the observed modulus values. As mentioned above, it is experimentally established that extracellular factors and the middle lamella contribute significantly to macro-scale mechanical responses [20–24]. Although we do not understand how much each of these extracellular factors contributes to the overall response, our experimental results suggest that, together, they can reduce the modulus value by approximately an order of magnitude.

*The plateau zone*

In tissue-scale experiments reported by Pieczykew and Zdunek [21] and Vanstreels et al. [58], an initial elastic response was followed by a transition zone, signifying a

non-linear stress–strain response caused by the initiation and occurrence of yielding or plastic deformation. In our subcellular-scale mechanical tests, the first linear zone was followed by a plateau zone, signifying a rapid reduction in stiffness due to permanent deformation that we assume was mediated by the collapse of certain structural features. This sharp decrease in the modulus value was unique to the subcellular-scale samples and was observed in all five samples within a strain range of 5–12 % and an applied stress range of 20–40 MPa (Fig. 6a). We refer to this stress–strain range as the critical stress–strain window, within which permanent structural failure occurs.

We assume that the 3D architecture at the cell boundary and the contribution of other surrounding cells through these cell boundaries may be why instantaneous collapse is not observed in tissue-scale mechanical tests. A tissue-scale sample, which is prepared by splitting open an onion epidermal cell wall profile, contains all the 3D features of a tissue with intact cells. It is mainly composed of outer periclinal walls attached to the surrounding walls by anticlinal walls through the middle lamella (Fig. 9). When a tissue strip is stretched, it imposes stress, which is distributed throughout the sample.

If we shift our focus to within a cell, a fragment of a cell wall with imaginary boundaries (Fig. 9, a black rectangle) is also stretched. However, the stress state of this fragment is affected and confounded by the stress states of the surrounding cells and of the anticlinal cell wall architecture [60]. Stretching this fragment in one direction should thin the sample in the other two directions, which is known in classical materials science as Poisson’s effect. In intact tissue, the thinning of a wall fragment at the cell boundary is restricted by complex 3D architecture. When a fragment of the wall is excised from a cell, the stress on the sample, including lateral thinning, is no longer restricted (Fig. 4a); the free edges of the samples can collapse through permanent structural change if the strain caused by stretching

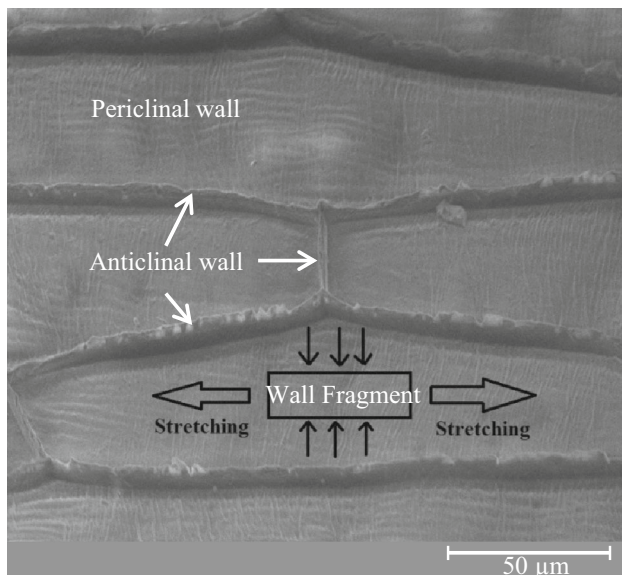


**Fig. 9** Split open onion epidermal cell wall profile, which represents half of a single layer of intact cells. The profile cell wall patch contains all the physical 3D features of a tissue

crosses the critical limit. Excising a cell wall fragment from tissue may also lead to a sample with shorter cellulose microfibrils. The *in vivo* length of cellulose microfibrils is still unknown but is assumed to be few micrometers (Kha et al. [41]). However, considering the tendency of cellulose microfibrils to aggregate [67], it is quite possible that a microfibril bundle could span a cell's entire width or even wrap around its whole 3D periphery. Along with their 3D architecture, long chains of cellulose microfibrils may also provide structural support to resist lateral collapse.

Our results suggest that the sharp drop in a sample's modulus value is accompanied by a large change in its lateral deformation (Fig. 7b). Similar to the three zones of the stress–strain plot, three zones of lateral strain were observed, but they were not observed for axial strain (Fig. 7a, b). Initially, to a certain point, the lateral strain remained very low and increased very slowly; this corresponds to the first linear zone of the stress–strain plot. After reaching a range of 12–15 %, lateral strain rose at a much higher rate, followed by another region with a low rate of change. The region with a high rate of change corresponds to the plateau zone, and the region with a slow rate of change corresponds to the second linear zone of the stress–axial strain plot (Fig. 7b).

The distinct plateau zone suggested that there is a critical range of stress and strain within which the plant cell wall architecture starts to irreversibly deform. Assuming that the first linear stress–strain zone represents the initial elastic response of the cell wall, the subsequent plateau in the stress–strain response represents the irreversible viscoelastic or plastic responses of the cell wall. Potential

causes of such non-linear responses include the separation of the interactions between the cellulose microfibrils and the matrix polymers, as well as the structural yielding of the matrix polymers. If the cell wall is considered to be a composite, the reinforcing cellulose microfibrils start to slide past the matrix polysaccharides within this critical range. If, as has been proposed more recently, the cell wall is considered to be an intricate network of structural polysaccharides and proteins, some irreversible structural failures occur in the system, promoting the rearrangement of the load-bearing constituents within this critical range. In either case, before reaching the critical range, all the structural constituents of the cell wall act and respond to a load as a single ensemble. Once the external load applied to the cell wall system crosses the critical strain energy limit, it is highly possible that the noncellulosic polysaccharides connecting the much stronger cellulose microfibrils would fail; the interactions between the noncellulosic polysaccharides are much weaker than those between the cellulose microfibrils, and that is where the strain energy is concentrated [42]. This concept is analogous to the behavior of biphasic materials, as discussed earlier, and the cell wall might loosen via cleavage of the components tethered between two cellulose microfibrils (Cosgrove [11]).

#### *The plateau zone and strain energy*

The energy required to induce irreversible cell wall deformation with an external load can be quantified by estimating the strain energy at the onset of the plateau zone. A quantitative understanding of the strain energy that a cell wall system can withstand before irreversible deformation occurs can be used as a critical tool to evaluate the types of interactions that cell wall structural constituents need to maintain structural integrity [68]. In classical mechanics, the total strain energy ( $U$ ) is defined in terms of stress ( $\sigma$ ), strain ( $\epsilon$ ), and volume ( $V$ ), which is given by the following equation [69]:

$$\text{Strain Energy, } U = \frac{1}{2} \sigma \epsilon V$$

Based on the average critical stress and strain values (stress 20–40 MPa, strain 5–12 %), we calculated that the amount of strain energy the cell wall can store before it reaches the critical zone is  $1.3 \text{ MJ m}^{-3}$ . This value is smaller than the  $4\text{--}40 \text{ MJ m}^{-3}$  reported by Thompson [68]. There are two reasons for this difference. First, Thompson [68] used the turgor-induced stress level of the cell wall (10–100 MPa), and this level can vary depending on the physical parameters of a cell. For example, the onion epidermal cell wall profile that we used for extracting cell wall samples had an average width ( $D$ ) of  $60 \text{ } \mu\text{m}$  and a thickness of ( $t$ )  $2 \text{ } \mu\text{m}$ . Based on a turgor pressure ( $P$ ) of  $1 \text{ MPa}$ ,

which is the maximum value suggested by Cosgrove [70], the hoop stress induced in these cells can be estimated as 15 MPa using the following equation:

$$\text{Hoop stress } (\sigma_h) = \frac{PD}{2t}$$

This value is much smaller than the 100 MPa that Thompson used in his calculation.

Second, the maximum strain value for an extensible tissue (40 %, Thompson [68]) incorporates both its elastic and plastic deformation stretching. When the cell wall begins plastic deformation, the origin of the energy required for further deformation can be very difficult to identify because it is related to the combination of architectural stability and rearrangement, as well as the deformation of each component. Thus, to use the strain energy to investigate the origin of cell wall deformation, it is more reliable to estimate the strain energy until the elastic limit, and then relate that energy to the cell wall's intact architectural network before the onset of permanent deformation or structural instability.

In our strain energy calculation, both of the aforementioned issues are resolved. We directly measure the stress on the cell wall material and consider it only up to the elastic limit. It is important to note that the average critical stress was 30 MPa, whereas the estimated turgor-induced stress was 15 MPa. These values suggest that the cell wall can withstand stress levels higher than that of maximum turgor. Thus, biochemical intervention through cell wall loosening is required for cell wall growth.

In addition, our calculated strain energy of  $1.3 \text{ MJ m}^{-3}$  is in good accordance with the cell wall's hydrogen energy density of  $2.1\text{--}4.3 \text{ MJ m}^{-3}$  (Thompson [68]). Even if only 50 % of the total hydrogen bonding energy participates in the connections between structural polysaccharides, our calculated strain energy suggests that hydrogen bonds alone might be sufficient to maintain the cell wall's structural integrity during growth.

#### *The second linear zone and its lower modulus value*

Similar to tissue-level experimental results, after the plateau zone, a second linear trend in the modulus value was observed for our subcellular-scale samples. However, as with the first linear zone, the average modulus value of  $143.9 \pm 72.4 \text{ MPa}$  was much higher than the tissue-scale experimental values of 3.86 and 5.63 MPa [21, 58]. The reasons for this difference are discussed above. However, the magnitude of the difference in modulus values for the two sample types was even higher in the second linear zone than in the first. The second linear zone follows the yield or plateau zone and is a zone of irreversible plastic deformation. Pectic polysaccharides, being highly dynamic [26]

and its tendency of responding faster to oscillation compared with other structural polysaccharides [50], it is reasonable to hypothesize that pectic polysaccharides will play a more dominant role in the irreversible zone, which is presumably characterized by the flexibility and flow-like behavior of the matrix polymers. In whole tissue, each cell is attached to other cells by the ML, which is primarily composed of pectic polysaccharides [28]. Thus, in the plastic deformation zone, intercellular adhesion may become more flexible, leading to a lower modulus value at the macroscopic scale. Along the same line, at the subcellular scale, the larger difference in modulus values might be expected because the samples were free from the effect of the ML.

In the subcellular-scale experiments, another important aspect observed in the second linear zone was the trend of gradually increasing modulus values (Fig. 6a, b). In tissue-scale experiments carried on the same material, the modulus values in this zone were either steady or gradually declined [21]. However, this increase in the modulus value in the large deformation zone is not unprecedented in the literature. Micromechanical tests of apple tissues are reported to produce sigmoidal stress–strain curves in which the modulus value increases with increasing strain [71, 72]. This trend is also found in biological tissues in which the internal structural constituents rearrange due to strain, leading to stiffening of the sample [73]. In our study, the increase in the modulus value that was observed in the second linear zone can also be related to the rearrangement of structural constituents in the plastic deformation zone.

Considering conservation of mass, the decrease in the volume of a cell wall sample (assuming constant thickness, this is equivalent to a decrease in area) during stretching can be related to the compaction of its structural constituents. By studying the instantaneous shape change of a typical sample over the entire loading process, two distinct areas were identified that were separated at the end of the plateau zone (Fig. 8b). Before the end of the plateau zone, the area of the sample was nearly the same, meaning that the axial expansion due to stretching was balanced by lateral contraction. At the initiation of the second linear zone, the surface area of the sample dropped sharply and then remained nearly the same until sample fracture. This decrease in surface area, which we suggest was caused by the compaction of cell wall structural polymers, was accompanied by a gradual increase in the modulus value. This phenomenon can be explained by the additional surface-to-surface interactions of closely compacted polymers, which would require more energy to slide past each other. This concept is similar to the turgor pressure-induced stiffening of cell wall material reported by Oey et al. [72]. As mentioned earlier, another reason could be that a change in the mechanical properties of a mechanically



stretched sample depends more on the failure of the matrix polymers; the axial strain followed an essentially linear trend (Fig. 8b), whereas the lateral strain followed a step-wise trend (Fig. 8b).

The increase in the modulus value at the end of the second linear zone, along with the recorded average lateral fracture strain of  $0.36 \pm 0.09$ , may also give insight into the amount of free space that is available for the lateral collapse of structural polysaccharides. The cellulose microfibrils in the onion epidermal cell wall are reported to be approximately 3 nm wide [52, 74]. Based on current cell wall models, if we consider the cellulose microfibrils to be separated and tethered by a xyloglucan and pectin network [10, 75], a 36 % lateral thinning due to microstructural failure of the matrix polymers requires at least 10.66 nm of free space between two neighboring cellulose microfibrils. Assuming that two cellulose microfibrils always have some space between them due to a hemicellulose coating [76], the required 10.66 nm of free space is in good agreement with the reported value of 20–40 nm between cellulose microfibrils in onion cell walls [77].

#### **The water-mediated mobility of cell wall matrix polymers may play a crucial role in the biophysical extensibility of the cell wall**

It is well established that the presence of water in the cell wall changes the mobility of its structural polysaccharides, and, consequently, its mechanical properties [19, 48, 51, 78, 79]. However, to the best of our knowledge, a quantitative investigation of the effect of moisture content on the cell wall's mechanical properties had not been reported in the literature. Water acts as a lubricating agent for the macromolecules of the cell wall [80], and some structural constituents, e.g., pectic polysaccharides, are more affected; they exhibit higher mobility than other polysaccharides in the presence of water [50, 51, 78]. The missing link is the proper understanding of the role that water molecules play in the biophysics and biomechanics of the cell wall under stress. As a soft biological material, the cell wall's biomechanical properties are sensitive to the rheological properties of its matrix [48]. This study attempted a quantitative study of water's contribution to the overall mechanics of the cell wall at the subcellular level, which is free from the variability that lies beyond the cell boundary. In whole tissue, cells are attached by the pectin-enriched ML, whose deformation and mobility are greatly affected by interactions with water. Therefore, the effect of water on tissue-scale samples may come more from the ML than the cell wall. Thus, by studying subcellular-scale samples without the ML layer, our results provide a better quantitative understanding of the contribution of water to the cell wall's mechanical properties. By testing non-dried, wet

samples without continuous hydration, we also attempted to create a state of intermediate water content lying between those of completely dry and continuously hydrated samples. The rationale behind considering non-dried, wet samples without continuous hydration as representative of an intermediate hydration state is as follows:

After removal from the water bath, the non-dried samples were placed on the MEMS device with access to surrounding water. However, as mentioned above, stiction was only activated when there was no water between the bottom of the sample and the test device's gripping surface. Thus, the samples were left without access to water only during experimentation, which lasted approximately 1 min. For a very small, subcellular-scale sample measuring  $123 \times 25 \times 2 \mu\text{m}$ , even 1 min might be sufficient for much of the water to evaporate from the samples. Due to the technical difficulty of examining microscale samples, our test setup was not equipped to measure water loss during experimentation. However, visual observations during the experiments suggested that samples of this size lost water very rapidly. For a  $2 \mu\text{m}$ -thin, subcellular-scale sample that is unaffected by the water state of the surrounding cells, this observation makes intuitive sense. Based on the absence of water access during experimentation and the quick-drying tendency of the microscale samples, the non-dried samples were considered to be in an intermediate water state between those of dry and continuously hydrated samples.

The moduli of elasticity (within the elastic linear zone) of subcellular-scale samples in three different water states were compared. For statistical analysis, the dry state data were taken from our previously published results (Zamil et al. [39]). As expected, the modulus values were significantly different between the three different states ( $p < 0.05$ ). Our goal was to quantify how much the modulus values changed within the elastic range due to the intervention of water. The average modulus values of completely hydrated, intermediately hydrated and completely dry samples within 2 % strain were  $0.44 \pm 0.12$ ,  $1.46 \pm 0.2$ , and  $3.72 \pm 0.82$  GPa, respectively. Between the completely hydrated and intermediate states, the modulus value increased 3.3-fold; between the intermediate and the dry states, the modulus value increased 2.5-fold.

We found that without a continuous supply of water, subcellular-scale cell wall samples lose water very quickly, leading to a significant increase in the stiffness value that falls within the range of the first elastic region, where no permanent structural collapse is expected. It is possible that, with access to water, the cell wall matrix polymers could weaken a cell wall under mechanical stress.

The critical stress limit (20–40 MPa) at which the continuously hydrated samples exhibited permanent structural failure (plateau zone) was not observed for samples

with intermediate hydration. This suggests that a sufficient supply of water is important for the irreversible plastic deformation of the cell wall, which manifested as the plateau zone seen in continuously hydrated samples.

## Conclusion

Primary plant cell wall samples that were longitudinally excised from onion outer epidermal profiles were characterized at the subcellular scale under two different hydration states. By modifying the MEMS-based tensile testing device reported previously by Zamil et al. [39] and by adapting a cryotome sectioning-based sample preparation technique, we were able to quantitatively characterize the cell wall, from no load to a large deformation range typically observed in non-dried tissue. A biphasic behavioral trend with two linear zones, which can also be seen at the tissue scale, was observed. However, the modulus values observed in both of the linear zones were at least one order of magnitude higher in our subcellular-scale samples than the values reported at the tissue scale. We also observed a plateau region that exhibited a sharp drop in the modulus value on the stress–strain plot, which was unique to subcellular-scale samples. From the plateau region, a critical stress (20–40 MPa) and strain (5–12 %) window was identified, within which we hypothesize that a major structural change occurs, leading to irreversible, plastic deformation. Before reaching the plateau zone, the cell wall can absorb  $1.3 \text{ MJ m}^{-3}$  of strain energy, which is in agreement with the hydrogen energy density observed in the cell wall. In the second linear zone of the biphasic stress–strain plot, the modulus value recovered, which may have resulted from the compaction of structural polysaccharides filling the free space in the non-deformed cell wall. Both of the aforementioned conclusions can be confirmed by incorporating molecular spectroscopy with the test protocol. The average modulus values in the first linear, plateau, and second linear zones were  $374.6 \pm 138.8$ ,  $112.6 \pm 69.9$ , and  $143.9 \pm 72.4$  MPa, respectively. An attempt was made to characterize subcellular-scale, non-dried samples using stiction as a gripping mechanism, which is novel in this field. However, stiction only allowed for the testing of samples with intermediate water content, and only up to 2 % strain, from which an average modulus value of  $1.46 \pm 0.2$  GPa was calculated. As expected, completely hydrated, intermediately hydrated, and completely dry cell wall modulus values were statistically significantly different ( $p < 0.05$ ); quantitatively, the modulus values increased 3.3- and 2.5-fold from lower to higher hydration states. The characterization of subcellular-scale samples provided important insights into the

architecture of primary plant cell walls that are not possible in tissue-scale experiments.

**Acknowledgements** This study was funded by the Center for Lignocellulose Structure and Formation, an Energy Frontier Research Center funded by the U. S. Department of Energy, Office of Science, Office of Basic Energy Sciences under Award Number DE-SC0001090.

## Compliance with Ethical Standards

**Conflict of interest** The authors declare that they have no conflict of interest.

## References

1. Keegstra K (2010) Plant cell walls. *Plant Physiol* 154:483–486. doi:[10.1104/pp.110.161240](https://doi.org/10.1104/pp.110.161240)
2. Park YB, Cosgrove DJ (2012) A revised architecture of primary cell walls based on biomechanical changes induced by substrate-specific endoglucanases. *Plant Physiol* 158:1933–1943
3. Harris PJ, Stone BA (2008) Chemistry and molecular organization of plant cell walls. *Biomass Recalcitrance*. Blackwell Publishing Ltd., pp 61–93
4. Caffall KH, Mohnen D (2009) The structure, function, and biosynthesis of plant cell wall pectic polysaccharides. *Carbohydr Res* 344:1879–1900. doi:[10.1016/j.carres.2009.05.021](https://doi.org/10.1016/j.carres.2009.05.021)
5. Burton RA, Gidley MJ, Fincher GB (2010) Heterogeneity in the chemistry, structure and function of plant cell walls. *Nat Chem Biol* 6:724–732
6. Albersheim P, Darvill A, Roberts K (2010) *Plant cell walls: from chemistry to biology*. Garland Science, Garland.
7. McCann M, Rose J (2010) Blueprints for building plant cell walls. *Plant Physiol* 153:365. doi:[10.1104/pp.110.900324](https://doi.org/10.1104/pp.110.900324)
8. Hepworth DG, Bruce DM (2004) Relationships between primary plant cell wall architecture and mechanical properties for onion bulb scale epidermal cells. *J Texture Stud* 35:586–602
9. Park YB, Cosgrove DJ (2012) Changes in cell wall biomechanical properties in the xyloglucan-deficient xxt1/xtt2 mutant of arabidopsis. *Plant Physiol* 158:465–475. doi:[10.1104/pp.111.189779](https://doi.org/10.1104/pp.111.189779)
10. Cosgrove D, Jarvis M (2012) Comparative structure and biomechanics of plant primary and secondary cell walls. *Front Plant Sci* 3:6
11. Cosgrove DJ (2005) Growth of the plant cell wall. *Nat Rev cell Biol* 6:850–861
12. Burgert I, Keplinger T (2013) Plant micro- and nanomechanics: experimental techniques for plant cell-wall analysis. *J Exp Bot* 64:4635–4649. doi:[10.1093/jxb/ert255](https://doi.org/10.1093/jxb/ert255)
13. Liepman AH, Wightman R, Geshi N et al (2010) Arabidopsis—a powerful model system for plant cell wall research. *Plant J* 61:1107–1121
14. Somerville C, Bauer S, Brininstool G et al (2004) Toward a systems approach to understanding plant cell walls. *Science* 306:2206–2211
15. McCann MC, Carpita NC (2008) Designing the deconstruction of plant cell walls. *Curr Opin Plant Biol* 11:314–320. doi:[10.1016/j.pbi.2008.04.001](https://doi.org/10.1016/j.pbi.2008.04.001)
16. Ryden P, Sugimoto-Shirasu K, Smith AC et al (2003) Tensile properties of arabidopsis cell walls depend on both a xyloglucan cross-linked microfibrillar network and rhamnogalacturonan II-borate complexes. *Plant Physiol* 132:1033–1040

17. Suslov D, Verbelen J-P, Vissenberg K (2009) Onion epidermis as a new model to study the control of growth anisotropy in higher plants. *J Exp Bot* 60:4175–4187
18. Keckes J, Burgert I, Fruhmant K et al (2003) Cell-wall recovery after irreversible deformation of wood. *Nat Mater* 2:810–813
19. Zabler S, Paris O, Burgert I, Fratzl P (2010) Moisture changes in the plant cell wall force cellulose crystallites to deform. *J Struct Biol* 171:133–141. doi:[10.1016/j.jsb.2010.04.013](https://doi.org/10.1016/j.jsb.2010.04.013)
20. Zdunek A, Umeda M (2005) Influence of cell size and cell wall volume fraction on failure properties of potato and carrot tissue. *J Texture Stud* 36:25–43
21. Pieczywek PM, Zdunek A (2014) Finite element modelling of the mechanical behaviour of onion epidermis with incorporation of nonlinear properties of cell walls and real tissue geometry. *J Food Eng* 123:50–59. doi:[10.1016/j.jfoodeng.2013.09.012](https://doi.org/10.1016/j.jfoodeng.2013.09.012)
22. Konstankiewicz K, Pawlak K, Zdunek A (2001) Influence of structural parameters of potato tuber cells on their mechanical properties. *Int Agrophys* 15:243–246
23. Waldron KW, Brett CT (2007) The role of polymer cross-linking in intercellular adhesion. In: Roberts JA, Gonzalez-Carranza Z (eds) *Plant cell separation and adhesion*. Blackwell Publishing Ltd, Ames, pp 183–204
24. Faisal T, Rey A, Pasini D (2013) A multiscale mechanical model for plant tissue stiffness. *Polymers (Basel)* 5:730–750. doi:[10.3390/polym5020730](https://doi.org/10.3390/polym5020730)
25. Höfte H, Peaucelle A, Braybrook S (2012) Cell wall mechanics and growth control in plants: the role of pectins revisited. *Front Plant Sci* 3:6
26. Dick-Pérez M, Zhang Y, Hayes J et al (2011) Structure and Interactions of plant cell-wall polysaccharides by two- and three-dimensional magic-angle-spinning solid-state NMR. *Biochemistry* 50:989–1000. doi:[10.1021/bi101795q](https://doi.org/10.1021/bi101795q)
27. Anderson CT, Carroll A, Akhmetova L, Somerville C (2010) Real-time imaging of cellulose reorientation during cell wall expansion in arabidopsis roots. *Plant Physiol* 152:787–796
28. Jarvis MC, Briggs SPH, Knox JP (2003) Intercellular adhesion and cell separation in plants. *Plant Cell Environ* 26:977–989
29. Gibson LJ (2012) The hierarchical structure and mechanics of plant materials. *J R Soc Interface* 9:2749–2766. doi:[10.1098/rsif.2012.0341](https://doi.org/10.1098/rsif.2012.0341)
30. Métraux J-P, Taiz L (1978) Transverse viscoelastic extension in Nitella I. Relationship to growth rate. *Plant Physiol* 61:135–138
31. Toole GGA, Gunning PA, Parker MML et al (2001) Fracture mechanics of the cell wall of Chara corallina. *Planta* 212:606–611. doi:[10.1007/s004250000425](https://doi.org/10.1007/s004250000425)
32. Sedighi-Gilani M, Sunderland H, Navi P (2005) Microfibril angle non-uniformities within normal and compression wood tracheids. *Wood Sci Technol* 39:419–430. doi:[10.1007/s00226-005-0022-0](https://doi.org/10.1007/s00226-005-0022-0)
33. Geitmann A (2006) Experimental approaches used to quantify physical parameters at cellular and subcellular levels. *Am J Bot* 93:1380–1390. doi:[10.3732/ajb.93.10.1380](https://doi.org/10.3732/ajb.93.10.1380)
34. Peaucelle A (2014) AFM-based Mapping of the elastic properties of cell walls: at tissue, cellular, and subcellular resolutions. e51317. doi:[10.3791/51317](https://doi.org/10.3791/51317)
35. Peaucelle A, Braybrook S, Le Guillou L et al (2011) Pectin-induced changes in cell wall mechanics underlie organ initiation in arabidopsis. *Curr Biol* 21:1720–1726
36. Kasas S, Longo G, Dietler G (2013) Mechanical properties of biological specimens explored by atomic force microscopy. *J Phys D Appl Phys* 46:133001
37. Kasas S, Gmur T, Dietler G (2008) The world of nano-biomechanics. 221–243. doi:[10.1016/B978-044452777-6.50014-0](https://doi.org/10.1016/B978-044452777-6.50014-0)
38. Notbohm J, Poon B, Ravichandran G (2012) Analysis of nanoindentation of soft materials with an atomic force microscope. *J Mater Res* 27:229–237
39. Zamil MS, Yi H, Haque A, Virendra MP (2013) Characterizing microscale biological samples under tensile loading: stress-strain behavior of cell wall fragment of onion outer epidermis. *Am J Bot* 100:1105–1115
40. Zamil MS, Yi H, Puri VM (2014) Mechanical characterization of outer epidermal middle lamella of onion under tensile loading. *Am J Bot* 101:778–787. doi:[10.3732/ajb.1300416](https://doi.org/10.3732/ajb.1300416)
41. Kha H, Tuble SC, Kalyanasundaram S, Williamson RE (2010) WallGen, software to construct layered cellulose-hemicellulose networks and predict their small deformation mechanics. *Plant Physiol* 152:774–786
42. Yi H, Puri VM (2012) Architecture-based multiscale computational modeling of plant cell wall mechanics to examine the hydrogen-bonding hypothesis of cell wall network structure model. *Plant Physiol* 160:1281–1292. doi:[10.1104/pp.112.201228](https://doi.org/10.1104/pp.112.201228)
43. Blewett J, Burrows K, Thomas C (2000) A micromanipulation method to measure the mechanical properties of single tomato suspension cells. *Biotechnol Lett* 22:1877–1883
44. Saito T, Soga K, Hoson T, Terashima I (2006) The bulk elastic modulus and the reversible properties of cell walls in developing quercus leaves. *Plant Cell Physiol* 47:715–725
45. Evered C, Majeবাদia B, Thompson DS (2007) Cell wall water content has a direct effect on extensibility in growing hypocotyls of sunflower (*Helianthus annuus* L.). *J Exp Bot* 58:3361–3371
46. Moore JP, Farrant JM, Driouich A (2008) A role for pectin-associated arabinans in maintaining the flexibility of the plant cell wall during water deficit stress. *Plant Signal Behav* 3:102–104
47. Hansen SL, Ray PM, Karlsson AO et al (2011) Mechanical properties of plant cell walls probed by relaxation spectra. *Plant Physiol* 155:246–258. doi:[10.1104/pp.110.166629](https://doi.org/10.1104/pp.110.166629)
48. Ulvskov P, Wium H, Bruce D et al (2005) Biophysical consequences of remodeling the neutral side chains of rhamnogalacturonan I in tubers of transgenic potatoes. *Planta* 220:609–620. doi:[10.1007/s00425-004-1373-8](https://doi.org/10.1007/s00425-004-1373-8)
49. Dick-Pérez M, Wang T, Salazar A et al (2012) Multidimensional solid-state NMR studies of the structure and dynamics of pectic polysaccharides in uniformly <sup>13</sup>C-labeled Arabidopsis primary cell walls. *Magn Reson Chem* 50:539–550. doi:[10.1002/mrc.3836](https://doi.org/10.1002/mrc.3836)
50. Wilson RH, Smith AC, Kačuráková M et al (2000) The mechanical properties and molecular dynamics of plant cell wall polysaccharides studied by fourier-transform infrared spectroscopy. *Plant Physiol* 124:397–406. doi:[10.1104/pp.124.1.397](https://doi.org/10.1104/pp.124.1.397)
51. White PB, Wang T, Park YB et al (2014) Water-polysaccharide interactions in the primary cell wall of arabidopsis thaliana from polarization transfer solid-state NMR. *J Am Chem Soc* 136:10399–10409. doi:[10.1021/ja504108h](https://doi.org/10.1021/ja504108h)
52. Zhang T, Mahgoudy-Louyeh S, Tittmann B, Cosgrove D (2014) Visualization of the nanoscale pattern of recently-deposited cellulose microfibrils and matrix materials in never-dried primary walls of the onion epidermis. *Cellulose* 21:853–862. doi:[10.1007/s10570-013-9996-1](https://doi.org/10.1007/s10570-013-9996-1)
53. Kaffle K, Xi X, Lee CM et al (2014) Cellulose microfibril orientation in onion (*Allium cepa* L.) epidermis studied by atomic force microscopy (AFM) and vibrational sum frequency generation (SFG) spectroscopy. *Cellulose* 21:1075–1086. doi:[10.1007/s10570-013-0121-2](https://doi.org/10.1007/s10570-013-0121-2)
54. Engqvist C, Forsberg S, Norgren M et al (2007) Interactions between single latex particles and silica surfaces studied with AFM. *Colloids Surf A* 302:197–203. doi:[10.1016/j.colsurfa.2007.02.032](https://doi.org/10.1016/j.colsurfa.2007.02.032)
55. Tas N, Sonnenberg T, Jansen H, Legtenberg R, Elwenspoek M (1996) Stiction in surface micromachining. *J Micromech Microeng* 6:385
56. Evert RF (2006) *Esau's pant anatomy*, 3rd edn. Wiley, New York, p 601

57. Hayles MF, Stokes DJ, Phifer D, Findlay KC (2007) A technique for improved focused ion beam milling of cryo-prepared life science specimens. *J Microsc* 226:263–269. doi:[10.1111/j.1365-2818.2007.01775.x](https://doi.org/10.1111/j.1365-2818.2007.01775.x)
58. Vanstreels E, Alamar MC, Verlinden BE et al (2005) Micromechanical behaviour of onion epidermal tissue. *Postharvest Biol Technol* 37:163–173
59. Sokolov I, Dokukin ME, Guz NV (2013) Method for quantitative measurements of the elastic modulus of biological cells in AFM indentation experiments. *Methods* 60:202–213. doi:[10.1016/j.ymeth.2013.03.037](https://doi.org/10.1016/j.ymeth.2013.03.037)
60. Zdunek A, Pieczywek PM (2013) Study on model development of plant tissue using the finite element method. *Inside Food Symposium*, Leuven, Belgium, pp 9–12
61. Lee T, Lakes RS (1997) Anisotropic polyurethane foam with Poisson's ratio greater than 1. *J Mater Sci* 32:2397–2401. doi:[10.1023/A:1018557107786](https://doi.org/10.1023/A:1018557107786)
62. Peel LD (2007) Exploration of high and negative Poisson's ratio elastomer-matrix laminates. *Phys status solidi* 244:988–1003. doi:[10.1002/pssb.200572717](https://doi.org/10.1002/pssb.200572717)
63. Greaves GN, Greer AL, Lakes RS, Rouxel T (2011) Poisson's ratio and modern materials. *Nat Mater* 10:823–837
64. Köhler L, Spatz H-C (2002) Micromechanics of plant tissues beyond the linear-elastic range. *Planta* 215:33–40. doi:[10.1007/s00425-001-0718-9](https://doi.org/10.1007/s00425-001-0718-9)
65. Spatz H, Köhler L, Niklas KJ (1999) Mechanical behaviour of plant tissues: composite materials or structures? *J Exp Biol* 202:3269–3272
66. Dintwa E, Jancsók P, Mebatsion HK et al (2011) A finite element model for mechanical deformation of single tomato suspension cells. *J Food Eng* 103:265–272. doi:[10.1016/j.jfoodeng.2010.10.023](https://doi.org/10.1016/j.jfoodeng.2010.10.023)
67. Donaldson L (2007) Cellulose microfibril aggregates and their size variation with cell wall type. *Wood Sci Technol* 41:443–460. doi:[10.1007/s00226-006-0121-6](https://doi.org/10.1007/s00226-006-0121-6)
68. Thompson DS (2005) How do cell walls regulate plant growth? *J Exp Bot* 56:2275–2285
69. Timoshenko S, Goodier JN (1984) *Theory of elasticity*, 3rd edn. Singapore, McGraw-Hill, Auckland
70. Cosgrove D (1997) Assembly and enlargement of the primary cell wall in plants. *Annu Rev Cell Dev Bi* 13:171–201
71. Alamar MC, Vanstreels E, Oey ML et al (2008) Micromechanical behaviour of apple tissue in tensile and compression tests: storage conditions and cultivar effect. *J Food Eng* 86:324–333
72. Oey ML, Vanstreels E, De Baerdemaeker J et al (2007) Effect of turgor on micromechanical and structural properties of apple tissue: a quantitative analysis. *Postharvest Biol Technol* 44:240–247. doi:[10.1016/j.postharvbio.2006.12.015](https://doi.org/10.1016/j.postharvbio.2006.12.015)
73. Decraemer WF, Maes MA, Vanhuysse VJ (1980) An elastic stress-strain relation for soft biological tissues based on a structural model. *J Biomech* 13:463–468. doi:[10.1016/0021-9290\(80\)90338-3](https://doi.org/10.1016/0021-9290(80)90338-3)
74. Davies LM, Harris PJ (2003) Atomic force microscopy of microfibrils in primary cell walls. *Planta* 217:283–289. doi:[10.1007/s00425-003-0979-6](https://doi.org/10.1007/s00425-003-0979-6)
75. Keegstra K, Albersheim P, Darvill A et al (2010) *Plant Cell Walls*. *Plant Physiol* 154:483–486. doi:[10.1104/pp.110.161240](https://doi.org/10.1104/pp.110.161240)
76. Hayashi T, Marsden MP, Delmer DP (1987) Pea xyloglucan and cellulose: V. Xyloglucan-cellulose interactions in vitro and in vivo. *Plant Physiol* 83:384–389
77. McCann MC, Wells B, Roberts K (1990) Direct visualization of cross-links in the primary plant cell wall. 96:323–334
78. Ha MA, Apperley DC, Jarvis MC (1997) Molecular rigidity in dry and hydrated onion cell walls. *Plant Physiol* 115:593–598
79. Vitré M, Sherwin HW, Driouich A et al (1999) Cell wall characteristics and structure of hydrated and dry leaves of the resurrection plant *Cratogeomys wilmsii*, a microscopical study. *J Plant Physiol* 155:719–726. doi:[10.1016/S0176-1617\(99\)80088-1](https://doi.org/10.1016/S0176-1617(99)80088-1)
80. Kačuráková M, Smith AC, Gidley MJ, Wilson RH (2002) Molecular interactions in bacterial cellulose composites studied by 1D FT-IR and dynamic 2D FT-IR spectroscopy. *Carbohydr Res* 337:1145–1153. doi:[10.1016/S0008-6215\(02\)00102-7](https://doi.org/10.1016/S0008-6215(02)00102-7)